Systems/Circuits

α_{2A}-Adrenergic Receptor Activation Decreases Parabrachial Nucleus Excitatory Drive onto BNST CRF Neurons and Reduces Their Activity *In Vivo*

Tracy L. Fetterly,[1,2] Aakash Basu,[1,3] Brett P. Nabit,[3] Elias Awad,[3] Kellie M. Williford,[1,2] Samuel W. Centanni,[1,2,3] Robert T. Matthews,[1,3] Yuval Silberman,[3,5] and Danny G. Winder[1,2,3,4,6,7]

[1]Vanderbilt Center for Addiction Research, [2]Vanderbilt Brain Institute, [3]Department of Molecular Physiology and Biophysics, [4]Vanderbilt J. F. Kennedy Center for Research on Human Development, Vanderbilt University School of Medicine, Nashville, Tennessee 37232-0615, [5]Department of Neural and Behavioral Sciences, Penn State College of Medicine, Hershey, Pennsylvania 17033-0850, [6]Department of Pharmacology, Vanderbilt University, and [7]Department of Psychiatry & Behavioral Sciences, Vanderbilt University Medical Center, Nashville, Tennessee 37232-0615

Stress contributes to numerous psychiatric disorders. Corticotropin releasing factor (CRF) signaling and CRF neurons in the bed nucleus of the stria terminalis (BNST) drive negative affective behaviors, thus agents that decrease activity of these cells may be of therapeutic interest. Here, we show that acute restraint stress increases cFos expression in CRF neurons in the mouse dorsal BNST, consistent with a role for these neurons in stress-related behaviors. We find that activation of α_{2A}-adrenergic receptors (ARs) by the agonist guanfacine reduced cFos expression in these neurons both in stressed and unstressed conditions. Further, we find that α- and β-ARs differentially regulate excitatory drive onto these neurons. Pharmacological and channelrhodopsin-assisted mapping experiments suggest that α_{2A}-ARs specifically reduce excitatory drive from parabrachial nucleus (PBN) afferents onto CRF neurons. Given that the α_{2A}-AR is a G_i-linked GPCR, we assessed the impact of activating the G_i-coupled DREADD hM4Di in the PBN on restraint stress regulation of BNST CRF neurons. CNO activation of PBN hM4Di reduced stress-induced *Fos* in BNST *Crh* neurons. Further, using *Prkcd* as an additional marker of BNST neuronal identity, we uncovered a female-specific upregulation of the coexpression of *Prkcd/Crh* in BNST neurons following stress, which was prevented by ovariectomy. These findings show that stress activates BNST CRF neurons, and that α_{2A}-AR activation suppresses the *in vivo* activity of these cells, at least in part by suppressing excitatory drive from PBN inputs onto CRF neurons.

Key words: BNST; CRF; norepinephrine; parabrachial; stress

Significance Statement

Stress is a major variable contributing to mood disorders. Here, we show that stress increases activation of BNST CRF neurons that drive negative affective behavior. We find that the clinically well tolerated α_{2A}-AR agonist guanfacine reduces activity of these cells *in vivo*, and reduces excitatory PBN inputs onto these cells *ex vivo*. Additionally, we uncover a novel sex-dependent coexpression of *Prkcd* with *Crh* in female BNST neurons after stress, an effect abolished by ovariectomy. These results demonstrate input-specific interactions between norepinephrine and CRF, and point to an action by which guanfacine may reduce negative affective responses.

Introduction

Stress is a major contributor to many psychiatric diseases, including depression, eating disorders, and addiction (Chrousos, 2009). Although the stress response is necessary for maintaining homeostasis in the body, chronic stress can become maladaptive over

Received April 23, 2018; revised Oct. 18, 2018; accepted Nov. 19, 2018.

Author contributions: T.L.F. wrote the first draft of the paper; T.L.F., B.P.N., K.M.W., S.W.C., R.T.M., Y.S., and D.G.W. edited the paper; T.L.F., K.M.W., Y.S., and D.G.W. designed research; T.L.F., B.P.N., E.A., K.M.W., S.W.C., R.T.M., and Y.S. performed research; T.L.F., A.B., E.A., K.M.W., and Y.S. analyzed data; T.L.F. and D.G.W. wrote the paper.

This work was supported by National Institutes of Health Grants R01DA042475 (D.G.W.), R01DA042475S1 (D.G.W.), R37AA019455 (D.G.W.), and R00AA022937 (Y.S.). Imaging and image data analyses were performed in part through the use of the Vanderbilt University School of Medicine Cell Imaging Shared Resource (supported by National Institutes of Health Grants CA68485, DK20593, DK58404, DK59637, and EY08126). We thank Elana Milano for technical assistance.

The authors declare no competing financial interests.

Correspondence should be addressed to either of the following: Dr. Yuval Silberman, Department of Neural and Behavioral Sciences, Penn State College of Medicine, 500 University Drive, P.O. Box 850, Mail Code H109, Hershey, PA 17033-0850, E-mail: yus72@psu.edu; or Dr. Danny G. Winder, Vanderbilt Center for Addiction Research, 23rd and Pierce Avenue South, Room 865A, Vanderbilt University School of Medicine, Nashville, TN 37232-0615, E-mail: danny.winder@vanderbilt.edu.

https://doi.org/10.1523/JNEUROSCI.1035-18.2018

 0270-6474/19/390472-13$15.00/0

time. The bed nucleus of the stria terminalis (BNST), a region within the extended amygdala, plays a critical role in physiological and behavioral responses to stress (Casada and Dafny, 1991; Sullivan et al., 2004; Crestani et al., 2013; Tran et al., 2014). Within the BNST, the corticotropin releasing factor (CRF) system is thought to promote negative affective responses to stress (Koob, 1999). BNST CRF signaling is enhanced following both acute and chronic stress exposure (Choi et al., 2006; Funk et al., 2006) and may be more stress reactive in females (Sterrenburg et al., 2012; Babb et al., 2013). Understanding the regulation of BNST CRF neurons during both acute and chronic stress could lead to better ways to address stress-induced pathologies.

Previous work has demonstrated an interaction between norepinephrine (NE) and glutamatergic inputs into the BNST (Egli et al., 2005; Shields et al., 2009; Flavin et al., 2014). However, the heterogeneity of BNST neurons remains a large obstacle in dissecting the impact of specific BNST inputs. We previously identified the parabrachial nucleus (PBN) as a functional glutamatergic input into the BNST that is sensitive to the clinically well tolerated α_{2A}-AR agonist guanfacine. Clinically, guanfacine has shown promise for the treatment of attention-deficit/hyperactivity disorder (Sallee et al., 2009). The PBN is known to form axosomatic synapses with BNST neurons, potentially allowing for increased influence over neuronal activity (Shimada et al., 1989; Dobolyi et al., 2005). Functionally, PBN projection neurons play a role in regulating many behaviors, including anxiety responses, fear conditioning, taste aversion, feeding, and pain sensitization (Carter et al., 2013, 2015; Sato et al., 2015; Chen et al., 2017; Campos et al., 2018). Here we find PBN afferents synapse onto BNST CRF cells, and that these CRF neurons are inhibited by α_{2A}-AR activation. Together, these studies suggest a role for the PBN in modulating stress activation of BNST CRF neurons.

In addition to addressing BNST heterogeneity using input specificity, postsynaptic markers can help to subdivide this complex region. In the central amygdala (CeA), CRF signaling has been shown to play a facilitating role in fear (Fadok et al., 2017; Sanford et al., 2017; Asok et al., 2018). Another CeA population is defined by the expression of protein kinase C δ (PKCδ); when activated, these cells have been shown to inhibit fear responses (Haubensak et al., 2010). Interestingly, there is relatively little cellular overlap between PKCδ and CRF in the CeA (Haubensak et al., 2010). Similarly, the BNST contains a population of PKCδ-expressing neurons, providing an additional marker to define BNST neurons.

In this study we assess the recruitment of BNST CRF cells following acute restraint stress, and explore regulation of these cells by guanfacine. We specifically investigate glutamatergic drive onto CRF neurons to provide insight into mechanisms that decrease stress activation of these neurons. Utilizing cFos as a marker of neuronal activation, we find that activation of α_{2A}-adrenergic receptors (ARs) can decrease the activation of BNST CRF neurons in both stressed and unstressed conditions. Further, we use electrophysiology to understand the modulation of glutamatergic drive onto these CRF neurons by the NE system. These studies provide a better understanding of the interaction between CRF and NE, two stress-recruited systems, in the BNST. Moreover, we found evidence of sex-dependent responses of BNST CRF cells based on postsynaptic alterations in marker expression. These insights will be important for future efforts in more effectively developing drugs that can alter maladaptive responses to stress.

Materials and Methods

Animals

Adult male and female C57BL/6J mice (>7 weeks of age; The Jackson Laboratory; RRID:IMSR_JAX:000664) were used for all fluorescence *in situ* hybridization studies. Ovariectomy and sham surgeries were performed by Jax Surgical Services (The Jackson Laboratory) at 6 weeks of age. CRF neurons were identified for electrophysiological analysis and immunohistochemistry experiments through the use of previously described male and female *CRF-tdtomato* reporter mice (Silberman et al., 2013). The *CRF-Cre* line used in these studies has been extensively evaluated and reliably reports CRF mRNA-expressing neurons (Chen et al., 2015). All mice were group housed (2–5 animals per cage) and maintained on a 12 h light/dark cycle (lights on 06:00–18:00) under controlled temperature (20–25°C) and humidity (30–50%) levels. Food and water were available *ad libitum*. All procedures were approved by the Institutional Animal Care and Use Committee at Vanderbilt University.

Restraint stress exposure

Mice were restrained during the light cycle (06:00–18:00) using 50 ml conical tubes (Fisher Scientific) altered to have holes throughout the tube and cap to allow for airflow (McElligott et al., 2010). Order of restraint was counterbalanced within experimental groups, to account for differences in time of day. Before undergoing restraint, mice were handled for 5 d as described previously (Olsen and Winder, 2010). Mice were allowed to acclimate to the test location in their home cage for 1 h in a sound- and light-attenuating box (Med Associates). During restraint, mice were placed inside separate sound- and light-attenuating boxes for 1 h before being returned to their home cage for 30 min. In some experiments, mice were treated with guanfacine (1 mg/kg, i.p.; Fisher Scientific) or clozapine-*N*-oxide (CNO; 3 mg/kg, i.p.) 30 min before restraint stress.

Fluorescent immunohistochemistry

Under isoflurane anesthesia, mice were transcardially perfused with 10 ml cold PBS followed by 20 ml 4% paraformaldehyde in phosphate buffered saline (PBS). Brains were extracted, postfixed for 24 h at 4°C in the same fixative, and then cryoprotected with 30% sucrose in PBS for a minimum of 48 h. Coronal sections were cut on a cryostat (Leica, CM3050S) at a thickness of 40 μm and stored in PBS before immunohistochemical staining. For cFos experiments, free-floating brain slices containing the BNST (bregma +0.14) were washed in PBS (4 × 10 min), permeabilized with 0.5% Triton X-100 in PBS (1 h), and then blocked with 5% normal donkey serum and 0.5% bovine serum albumin (1 h); all steps were at room temperature. Sections were then incubated in cFos primary antibody (1:2000; sc-52, Santa Cruz Biotechnology; RRID:AB_2106783) in blocking solution for 24 h at room temperature. Slices then underwent PBS washes (4× 10 min) followed by incubation in donkey AlexaFluor 488 anti-rabbit (1:500; Jackson ImmunoResearch; RRID:AB_2313584) fluorescent dye-conjugated secondary antibody for 24 h at 4°C in PBS with 0.1% Triton X-100. Slices were then washed with PBS (4× 10 min), mounted on positively charged slides (Fisher Scientific), and coverslipped with PolyAquamount (Polysciences) when dry. Modifications were made to the staining protocol for visualizing calcitonin gene-related peptide (CGRP) terminals surrounding CRF cells in CRF-tdtomato mice, including an altered blocking buffer (10% normal donkey serum), primary incubation step in CGRP primary antibody (1:400; ab36001, Abcam; RRID:AB_725807) for 3 d at 4°C, and secondary amplification using donkey Cy5 anti-goat (1:400; Jackson ImmunoResearch; RRID:AB_2340415) overnight at 4°C. For visualizing DREADD viral injection sites, no amplification steps were used. Images of injections sites and antibody-labeled tissue were obtained using a Zeiss 710 scanning confocal microscope and a 20×/0.75 NA lens, keeping acquisition parameters consistent within an experiment. For cFos cell quantification, the number of cFos+ cells per dorsal BNST (dBNST) was averaged over two coronal slices. For ChR2 injection verification (without amplification), images were obtained using an Olympus SZX12 stereo microscope. Images were analyzed using ImageJ software (NIH; RRID:SCR_003070), with the same brightness and contrast settings applied across all images.

RNA in situ *hybridization*

Fluorescence *in situ* hybridization assays were performed using the RNAScope Fluorescent Multiplex Reagent Kit (Advanced Cell Diagnostics) to visualize RNA transcripts in BNST coronal sections. Probes used include Mm-Crh-C1, Mm-Fos-C2, and Mm-Prkcd-C3. Mice were put under isoflurane anesthesia and brains were quickly extracted, submerged in ice-cold, oxygenated (95% O_2/5% CO_2) artificial CSF (ACSF) containing the following (in mM[SCAP]): 124 NaCl, 4.4 KCl, 2.5 $CaCl_2$, 1.3 $MgSO_4$, 1 NaH_2PO_4, 10 glucose, 26 $NaHCO_3$, and flash-frozen in Optimal Cutting Temperature Solution (VWR) using Super Friendly Freeze-It Spray (Fisher Scientific). Embedded brains were stored at −80°C before being cut on a cryostat (Leica, CM3050S). Slices (16 μm) were adhered to charged slides (Denville Scientific) and immediately frozen with dry ice and stored at −80°C until staining. Fixation, dehydration, hybridization, and staining protocols for fresh frozen tissue were performed according to ACD's online specifications. *Z*-stack BNST images were obtained with a 63×/1.4 NA oil lens on a Zeiss 710 scanning confocal microscope. Three images were taken to cover the dorsal, medial, and lateral areas of the dorsal BNST (bregma +0.14). Negative control images (negative control probe: DapB) were used to determine brightness and contrast parameters for experimental images. Max intensity projections were used for analysis with ImageJ software (NIH). Counts were combined for the three BNST regions and then averaged with the counts for the contralateral BNST in the slice. Transcripts were identified as individual dots within a cell, using DAPI-labeled nuclei to identify individual cells. A blinded reviewer identified cells as positive for zero, one, two, or three of the following transcripts: *Crh*, *Prkcd*, *Fos*. Negative control images were used to determine thresholding parameters that excluded nonspecific fluorescence.

Microinjection surgeries

Mice that were >6 weeks of age were used for viral injections studies. Mice were anesthetized with isoflurane and injected intracranially with AAV constructs expressing either ChR2 or DREADD as described below. For the optical stimulation experiments, 200–300 nl of AAV5-CaMKIIα-ChR2:YFP (University of North Carolina Viral Vector Core) was injected at 40 nl/min into one of three regions based on coordinates from the Franklin and Paxinos (2007) mouse brain atlas: insula (AP: 0.02, ML: ±3.66, DV: −4.30), mPFC (AP: 1,78, ML: ±0.22, DV: −2.91), and PBN (AP: −5.34, ML: ±1.31, DV: −4.30; 15.03° angle). For both the restraint stress and electrophysiological control DREADD experiments, 200–300 nl of AAV5-hSyn-hM4D(Gi)-mCherry (Addgene) was injected at 40 nl/min into the PBN (coordinates above). Mice were treated with 5 mg/kg of ketoprofen once every 24 h for 48 h following surgery. Virally injected mice were killed 6–12 weeks after surgery for anatomical and electrophysiological analysis.

Electrophysiology

Brain slice preparation. Brain slices containing the BNST (bregma +0.14–0.26) were prepared from adult CRF-tdtomato reporter mice as previously described (Nobis et al., 2011; Silberman et al., 2013; Flavin et al., 2014). Briefly, mice were allowed to acclimate in their home cage for 1 h in a sound- and light-attenuating box (Med Associates). Following acclimation, mice were anesthetized with isoflurane and brains were quickly removed and submerged in ice-cold, oxygenated low sodium sucrose dissecting solution (in mM: 194 sucrose, 20 NaCl, 4.4 KCl, 2 $CaCl_2$, 1 $MgCl_2$, 1.2 NaH_2PO_4, 10 glucose, 26 $NaHCO_3$). A vibratome (Leica) was used to prepare coronal brain slices (300 μm). Slices were transferred to a holding chamber containing oxygenated ACSF and allowed to recover for 1 h.

Whole-cell, voltage-clamp recordings. All electrophysiology recordings were made using Clampex 9.2–10.3 and analyzed using Clampfit 10.2–10.7 (Molecular Devices). Whole-cell, voltage-clamp recordings of AMPA receptor-mediated EPSCs were made at −70 mV and pharmacologically isolated by the addition of 25 μM picrotoxin (Tocris Bioscience) to the ACSF (described above). Recording electrodes for electrical stimulation experiments were filled with the following (in mM): 118 CsOH, 117 D-gluconic acid, 5 NaCl, 10 HEPES, 0.4 EGTA, 2 $MgCl_2$, 5 tetraethylammonium chloride, 4 ATP, 0.3 GTP, pH 7.2–7.3, 280–290 mOsm. Recording electrodes for optical stimulation experiments were filled with the folloiwng (in mM): 135 K^+-gluconate, 5 NaCl, 2 $MgCl_2$, 10 HEPES, 0.6 EGTA, 4 ATP, 0.4 GTP, pH 7.2–7.3, 280–290 mOsm. Electrical stimulation occurred for 1 ms every 30 s and a 50 ms inter-event interval was used to assess paired-pulse ratio (PPR). Optical stimulation was under the control of a T-Cube LED Driver (LEDD1B, Thorlabs) and passed through an EN-GFP filter cube (Olympus) to produce blue wavelength light. Stimulation occurred for 5 ms every 20 s. The presence of ChR2 in each slice was confirmed via fluorescence, but viral expression was not quantified. Instead, initial optical EPSCs (oEPSCs) were adjusted so that all baseline oEPSCs were between 100 and 300 pA. Neutral density filters and microscope apertures were adjusted to achieve this baseline amplitude. Data are represented as average amplitude of three sweeps, with amplitudes normalized to baseline oEPSC amplitude. For both electrical and optical stimulation, experiments in which the access resistance changed by >20% were not included in the data analyses. Access resistance was monitored via a voltage step occurring in between each sweep. Recordings were made using a 10 kHz sampling rate and a 4 kHz low-pass filter.

Statistical analysis

All data are represented as mean ± SEM except for when SD is used to address within-cell variability of latency to respond to optical stimulation. We used both male and female mice throughout the study. When sex was not found to be a statistically significant variable, we have combined male and female data for analysis. For the immunohistochemistry experiments a two-way ANOVA was used to assess stress and guanfacine effects. *Post hoc* analysis was performed using Tukey's multiple-comparisons test. For all RNA *in situ* experiments, two-way ANOVAs were used to assess effect of both treatment and sex. When both factors (or an interaction) were found to have a significant effect, Tukey's multiple-comparison test was used to make multiple comparisons. When there was no significant effect of sex, Sidak's multiple-comparisons test was used to make comparisons within treatment groups for each sex. For electrophysiological experiments, paired *t* tests were used to assess drug effects on amplitude and PPR. Unpaired *t* tests were used to compare oEPSC kinetics between insula and PBN inputs as well as to compare the effects of CNO on EPSC amplitude in control and hM4Di-expressing animals. Statistical analyses were performed using GraphPad Prism 7.

Reagents

All reagents used were purchased from Millipore Sigma unless otherwise noted in the text. For *in vivo* experiments, all drugs were diluted in sterile saline (0.9% sodium chloride; Hospira). For electrophysiological experiments, all drugs were diluted in diH_2O to make stock solution (10 mM) except for picrotoxin (diluted in DMSO) and norepinephrine (added directly to ACSF).

Results

cFos expression in BNST CRF neurons is increased by restraint stress and decreased by systemic administration of the α_{2A}-AR agonist guanfacine

As an index of neuronal activity in the dBNST we used immunohistochemistry to identify neurons expressing cFos following an acute restraint stress (Fig. 1*a*). We found that cFos expression is significantly increased after restraint stress when compared with the control no-stress condition (Fig. 1*b*,*c*). Analysis via one-way ANOVA shows a significant effect of time after restraint stress ($F_{(4,10)} = 19.57$, $p < 0.001$). *Post hoc* analysis with Dunnett's multiple-comparison test reveals that cFos is significantly increased relative to the no stress control (12.9 ± 4.3 cells/dBNST) at 30 min (39.8 ± 1.3 cells/dBNST, $p < 0.001$), 1 h (37.1 ± 2.3 cells/dBNST, $p < 0.001$), and 2 h (25.1 ± 2 cells/dBNST, $p = 0.028$) after restraint stress, but is no longer significantly increased after 4 h (17.8 ± 2.4 cells, $p = 0.53$).

To look specifically at restraint stress activation of CRF cells, we used both a fluorescent *in situ* hybridization assay (Fig. 1*e*)

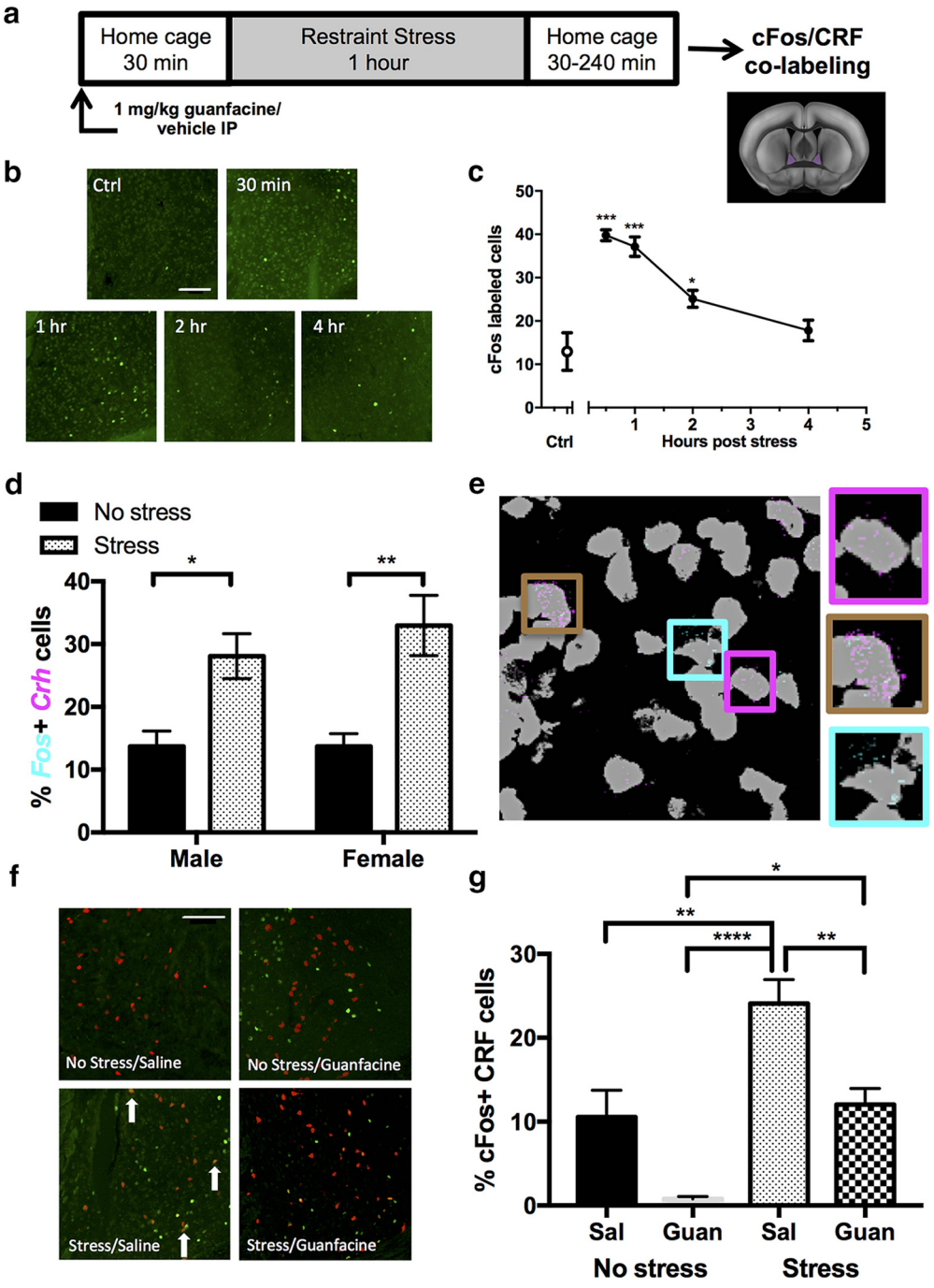

Figure 1. Restraint stress induces transient cFos expression in BNST CRF neurons in an α_{2A}-AR sensitive manner. ***a***, Schematic showing timeline of animal injection, restraint stress, and *in situ* hybridization/immunohistochemistry assays, along with image of coronal section with the dBNST highlighted (purple) to denote region used for analysis throughout. ***b***, Representative images of cFos labeling in the dBNST showing control, 30 min, 1 h, 2 h, and 4 h ± SEM time points after restraint stress. Scale bar, 100 μm. ***c***, Summary data showing the mean ± SEM number of cFos-labeled cells in dBNST sections from control conditions or at various time points following a 1 h restraint stress. $n = 3$ male mice/group. *Indicates significant difference from control conditions (***$p < 0.001$, *$p < 0.05$). ***d***, Summary bar graph showing the percentage of *Crh* neurons that express *Fos* 30 min after restraint stress in male and female mice. Males: no stress $n = 5$, stress $n = 5$; Females: no stress $n = 5$, stress $n = 4$. *Indicates significant difference between stress conditions (*$p < 0.05$, **$p < 0.01$). ***e***, Example image of RNA *in situ* assay (gray, DAPI-labeled nuclei; magenta, *Crh* transcripts; cyan, *Fos* transcripts). Boxes provide magnified examples of cells expressing one or both transcripts (magenta, *Crh*; brown, *Crh/Fos*; cyan, *Fos*). ***f***, Representative fluorescent immunohistochemical images of merged cFos (green) and CRF (red) labeling in the dBNST 30 min after restraint stress for no stress/saline, no stress/guanfacine, stress/saline, and stress/guanfacine conditions. Scale bar, 100 μm. ***g***, Summary bar graph showing the mean ± SEM percentage of cFos+ CRF neurons 30 min after restraint stress for the following conditions: no stress/saline ($n = 9$; 6 male/3 female), no stress/guanfacine ($n = 6$; 4 male/2 female), stress/saline ($n = 8$; 5 male/3 female), stress/guanfacine ($n = 9$; 4 male/5 female). *Indicates significant difference compared with each other group (*$p < 0.05$, **$p < 0.01$, ***$p < 0.001$, ****$p < 0.0001$).

and a well validated previously used CRF-tdtomato reporter mouse (Silberman et al., 2013; Chen et al., 2015) to quantify colocalization of cFos with dBNST CRF neurons using immunohistochemistry (Fig. 1*f*). We found similar increases in the percentage of cFos+ CRF neurons following restraint stress in both assays (Fig. 1*d*,*g*). For the RNA *in situ* assay (Fig. 1*d*), a two-way ANOVA shows a significant effect of stress on the percentage of *Crh* cells that express *Fos* ($F_{(1,15)} = 27.18$, $p < 0.001$), but no effect

of sex ($F_{(1,15)} = 0.57$, $p = 0.462$) and no interaction between the variables ($F_{(1,15)} = 0.57$, $p = 0.46$). Sidak's multiple-comparisons test shows a significant increase in *Fos*+ *Crh* neurons in both males (no stress: 13.7 ± 2.4%; stress: 28.1 ± 3.6%; $p = 0.011$) and females (no stress: 13.7 ± 2.1%; stress: 33.0 ± 4.8%; $p = 0.002$).

Previous work has shown that administration of α_{2A}-AR agonists systemically, or directly into the BNST, can inhibit CRF-dependent behaviors such as drug withdrawal-related phenotypes and stress-induced reinstatement of drug seeking behavior (Shaham et al., 2000; Wang et al., 2001; Mantsch et al., 2010). Further, α_{2A}-AR activation in the BNST is able to decrease excitatory drive (Shields et al., 2009; Flavin et al., 2014). Thus, we wanted to assess the impact the α_{2A}-AR agonist guanfacine (1 mg/kg) on the activity of CRF neurons (Fig. 1*f*,*g*). A two-way ANOVA showed a significant effect of guanfacine ($F_{(1,28)} = 17.71$, $p = 0.0002$) and stress ($F_{(1,28)} = 22.94$, $p < 0.0001$), but no significant interaction ($F_{(1,28)} = 0.20$, $p = 0.657$). A *post hoc* analysis using Tukey's multiple-comparisons test shows a significant increase in cFos+ CRF neurons following restraint stress (no stress, saline: 10.5 ± 3.2%; stress, saline: 24.1 ± 2.8%; $p = 0.003$). Treatment with guanfacine before restraint stress results in a significantly lower percentage of cFos+ CRF neurons compared with saline-treated stress animals (stress, guanfacine: 12.0 ± 1.9%; $p = 0.009$). Additionally, treatment with guanfacine in the no stress condition significantly decreased cFos+ CRF neurons compared with the guanfacine/stress condition (no stress, guanfacine: 0.7 ± 0.3%; $p = 0.030$). Together these data show that acute restraint stress results in transient cFos activation in CRF neurons, and that cFos expression in CRF neurons can be reduced by treatment with guanfacine.

Norepinephrine inhibits glutamatergic transmission onto CRF neurons via α-AR activation

In previous studies, we and others have found that activation of noradrenergic receptors can regulate excitatory drive in unidentified neuronal populations in the dorsal BNST (Krawczyk et al., 2011; Nobis et al., 2011; Flavin et al., 2014). To better understand the interaction between NE signaling and BNST CRF neuron activation, we examined the actions of NE and agonists for both α- and β-ARs in modulating excitatory drive onto CRF neurons in *ex vivo* BNST slices. We recorded from tdtomato+ neurons in the BNST of CRF reporter mice and evoked glutamatergic EPSCs by electrical stimulation in the presence of picrotoxin. A paired *t* test shows that 10 min bath application of 1 μM NE significantly inhibited EPSC amplitude (−42.5 ± 8.7% change from baseline, $p = 0.008$; Fig. 2*a*) without significantly altering the PPR of the EPSCs (+8.3 ± 9.8% change from baseline, $p = 0.44$). To further dissect NE signaling, we then repeated the electrical stimulation experiment using agonists for α_1-, α_{2A}-, and β-ARs (Fig. 2*b–d*). A paired *t* test shows that, similar to NE, bath application of 100 μM methoxamine (α_1-AR agonist) significantly inhibits EPSC amplitude (−26.0 ± 7.3% change from baseline, $p = 0.10$; Fig. 2*b*) without significantly altering PPR (−1.5 ± 5.3% change from baseline, $p = 0.56$). A paired *t* test shows that bath application of 1 μM guanfacine (α_{2A}-AR agonist) also significantly inhibited EPSC amplitude (−60.5 ± 4.7% change from baseline, $p < 0.0001$; Fig. 2*c*), while also significantly increasing PPR (+32.7 ± 5.7% change from baseline, $p < 0.001$). Finally, a paired *t* test shows that bath application of 3 μM isoproterenol (β-AR agonist) significantly increases EPSC amplitude (+28.8 ± 7.2% change from baseline, $p = 0.007$; Fig. 2*d*) without altering PPR (−6.7 ± 5.0% change from baseline, $p = 0.15$).

Based on the ability of systemic guanfacine to decrease stress-induced cFos in CRF cells in our previous experiments, we further focused on the actions of α_{2A}-AR signaling using the antagonist atipamezole (1 μM). *Ex vivo* BNST slices were pretreated with atipamezole before bath application of 1 μM NE, with the antagonist remaining in the bath for the duration of the experiment. The time course shown in Figure 2*f* demonstrates that atipamezole is able to block the effects of NE on excitatory drive. A paired *t* test shows that in the presence of atipamezole, bath application of 1 μM NE no longer significantly inhibits EPSC amplitude (+21.3 ± 11.7% change from baseline, $p = 0.143$; Fig. 2*g*) and PPR remains unaltered (−1.1 ± 6.4% change from baseline, $p = 0.940$).

Input-specific NE action on excitatory control of BNST CRF neurons

We next used *ex vivo* channelrhodopsin assisted circuit mapping to begin to determine regions that provide excitatory input to BNST CRF neurons, examining the PBN and insular cortex (McDonald et al., 1999; Dobolyi et al., 2005). AAV5-CaMKIIα-ChR2-YFP was stereotaxically injected into the region of interest in CRF reporter mice (Fig. 3*a*) and allowed to express for at minimum 6 weeks before preparing slices for electrophysiology. After verifying ChR2 expression in terminals in the BNST via visual inspection, we recorded from tdtomato+ neurons in the BNST and used full-field blue-light stimulation to evoke oEPSCs in the presence of picrotoxin. For each cell recorded from, we noted the presence or absence of an oEPSC, and in the case of cells that responded, continued to stimulate every 20 s for 10 min to allow for response kinetics analysis. The PBN and insula exhibited different response profiles (Fig. 3*b*): insular cortex afferent stimulation led to a reliable response in CRF neurons (87% of cells responded, 20/23 cells), whereas PBN afferent stimulation resulted in an intermediate phenotype (50% of cells responded, 14/28 cells). Immunohistochemistry staining of CGRP in the BNST as a marker for the PBN input (Shimada et al., 1989) provides further anatomical support of this intermediate phenotype, as some but not all CRF cell somas are surrounded by CGRP+ terminals (Fig. 3*c*).

Having identified the insular cortex and PBN as providing excitatory input to BNST CRF neurons, we next analyzed the response kinetics of recorded oEPSCs from these inputs (Fig. 3*d*). Unpaired *t* tests show that oEPSCs resulting from insula terminal stimulation compared with PBN terminal stimulation have a significantly greater latency to peak following optical stimulation (PBN: 11.51 ± 0.96 ms; insula: 15.25 ± 1.04 ms; $p = 0.03$), while showing less variability in latency to respond between sweeps within a cell (PBN: SD = 1.84 ms; insula: SD = 1.03 ms). Additionally, the decay time of insular input oEPSCs was significantly longer (PBN: 11.63 ± 1.99 ms; insula: 18.73 ± 1.79 ms; $p = 0.023$). Rise time was not significantly different between the two (PBN: 3.8 ± 0.7 ms; insula: 4.57 ± 0.43 ms; $p = 0.342$).

Next, we determined whether NE could modulate these inputs as seen in the electrical stimulation experiments. The same optical stimulation set-up was used as described for the mapping experiments, but now AR agonists were bath applied during stimulation (Fig. 3*e*,*f*). A paired *t* test (Fig. 3*h*) shows that 20 min bath application of 1 μM NE significantly inhibits oEPSC amplitude when stimulating PBN afferents (−44.3 ± 9.4% change from baseline, $p = 0.018$), whereas not altering oEPSC amplitude during insular stimulation (−4.2 ± 3.7% change from baseline, $p = 0.341$). This demonstrates that al-

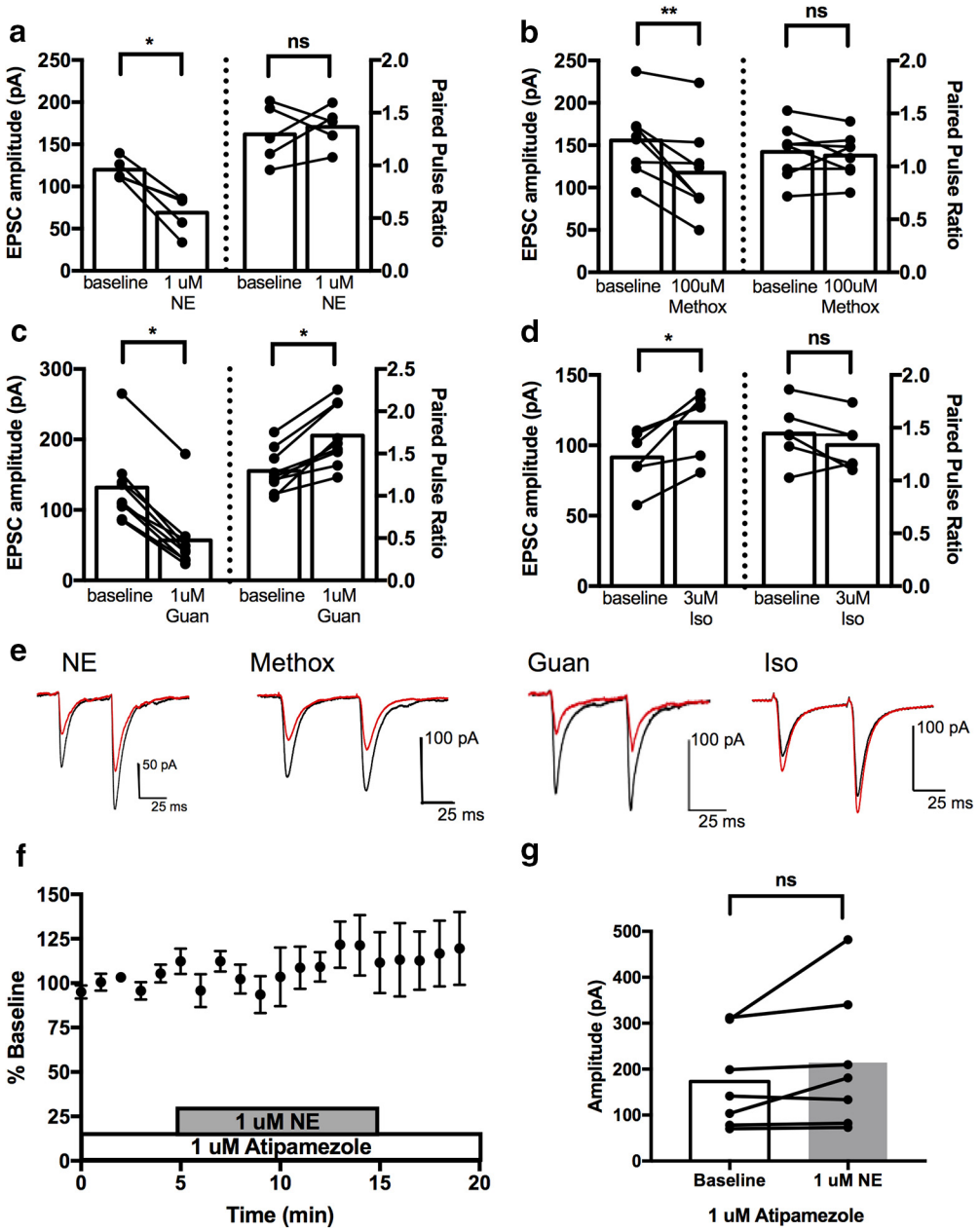

Figure 2. NE regulation of excitatory drive onto CRF neurons is mediated by α-AR signaling and can be blocked by the of α_{2A}-AR antagonist atipamezole. ***a–d***, Bar graphs summarizing the effects of AR agonists on EPSC amplitude (left) and PPR (right) in BNST CRF neurons. ***a***, Effects of NE ($n = 5$ cells, $N = 3$ male mice). ***b***, Effects of α_1-AR agonist methoxamine (Methox; $n = 8$ cells, 4 male mice). ***c***, Effects of α_{2A}-AR agonist guanfacine (Guan; $n = 5$ cells, $N = 3$ male mice). ***d***, Effects of β-AR agonist isoproterenol (Iso; $n = 6$ cells, $N = 3$ male mice) *Indicates significant difference compared with baseline (*$p < 0.05$). ***e***, Representative EPSC traces before (black) and after (red) AR agonist application. ***f***, Time course showing effects of pretreatment with α_{2A}-AR antagonist atipamezole on NE modulation of EPSC amplitude in BNST CRF neurons, graphed as a ±SEM. ***g***, Bar graph comparing EPSC amplitude during atipamezole pretreatment before and after NE application ($n = 7$ cells, $N = 1$ male, 3 female mice).

though both regions send glutamatergic inputs to BNST CRF neurons, only the PBN input is sensitive to regulation by NE. Having shown the effects of NE in the electrical stimulation experiments to be mediated by α_{2A}-AR signaling, we also tested the effect of guanfacine on PBN afferent stimulation-evoked oEPSCs (Fig. 3*g*). A paired *t* test (Fig. 3*h*) shows that 20 min bath application of 1 μM guanfacine significantly reduces oEPSC amplitude similar to NE application (−40.0 ± 11.5% change from baseline, $p = 0.026$). This provides further support for the role of α_{2A}-AR signaling in mediating CRF neuronal activity in the BNST.

Activation of PBN hM4Di blunts stress-induced Fos

Having identified the PBN as a guanfacine-sensitive glutamatergic input to BNST CRF neurons, we next wanted to determine whether manipulating the activity of this input could alter the restraint stress-induced *Fos* response in a manner similar to systemic guanfacine administration. To do this we used a chemogenetic strategy through the use of the hM4Di DREADD, which couples to Gi-signaling as the α_{2A}-AR does to mimic activation of the α_{2A}-AR by guanfacine. AAV5-hSyn-HA-hM4D(Gi)-mCherry was stereotaxically injected bilaterally into the PBN and given at least 3 weeks for expression to occur (Fig. 4*d*). To verify

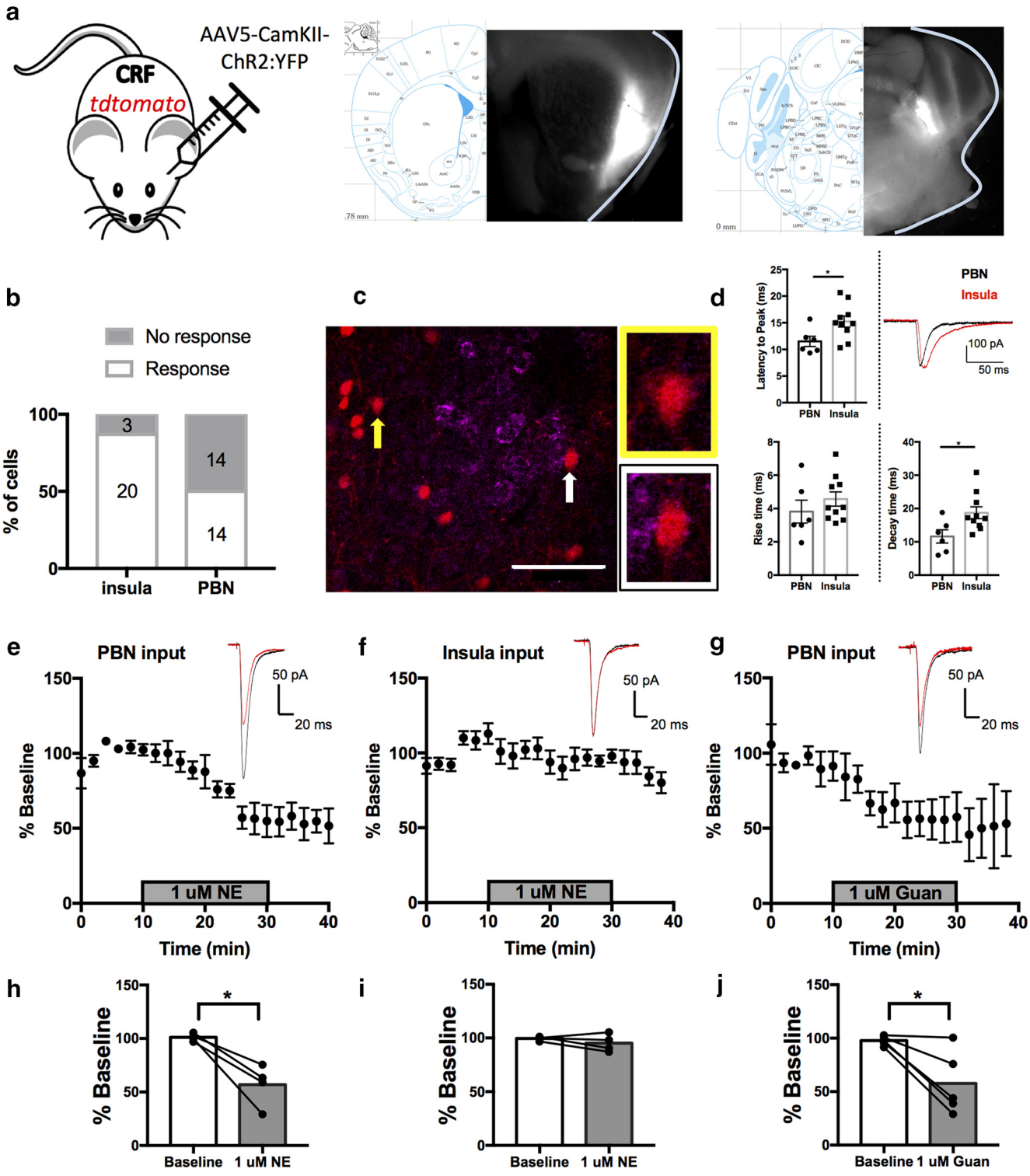

Figure 3. BNST CRF neurons receive kinetically distinct excitatory input from both the insular cortex and PBN, but the PBN input can be regulated by both NE and guanfacine. ***a***, Illustrated mouse indicating that for Figure 3, *CRF-tdtomato* reporter mice were stereotaxically injected with AAV5-CaMKIIα-ChR2:YFP, along with example stereo microscope images of injection sites for insular cortex and PBN. ***b***, Summary of percentage of BNST CRF cells that respond to insula or PBN activation. ***c***, Representative image of CGRP labeling (purple; marking PBN input) around BNST CRF neurons (red) demonstrating CRF cells surrounded by CGRP (white arrow; white box: magnified image of cell) and CRF cells without PBN input (yellow arrow; yellow box: magnified image of cell). Scale bar, 50 μm. ***d***, Bar graphs comparing oEPSC kinetics between PBN ($n = 6$ cells, female mice) and insula ($n = 10$ cells, female mice) stimulation. Top left, Latency to oEPSC peak (ms). Top right, Representative oEPSC traces from insula (red) and PBN (black). Bottom left, Rise time (10 –90%) of oEPSC (ms). Bottom right, Decay time (90 –10%) of oEPSC (ms). *Indicates significant difference using unpaired *t* test (*$p < 0.05$). ***e***, ***f***, Summary graphs showing effect of NE on oEPSC amplitude, graphed as percentage of baseline, for PBN stimulation (d; $n = 4$, $N = 3$ female mice) and insula stimulation (e; $n = 4$, $N = 4$ female mice). Inset, Representative oEPSC traces before (black) and after (red) NE application. ***g***, Summary graph showing effect of guanfacine on oEPSC amplitude, graphed as percentage of baseline, for PBN stimulation ($n = 5$, 2 male mice, $N = 2$ female mice). Inset, Representative oEPSC traces before (black) and after (red) guanfacine application. ***h***–***j***, Bar graphs comparing average oEPSC amplitude, graphed as percentage of baseline, 5 min before and after drug wash-on. *Indicates significant difference using paired *t* test (*$p < 0.05$). All data are represented as mean ± SEM.

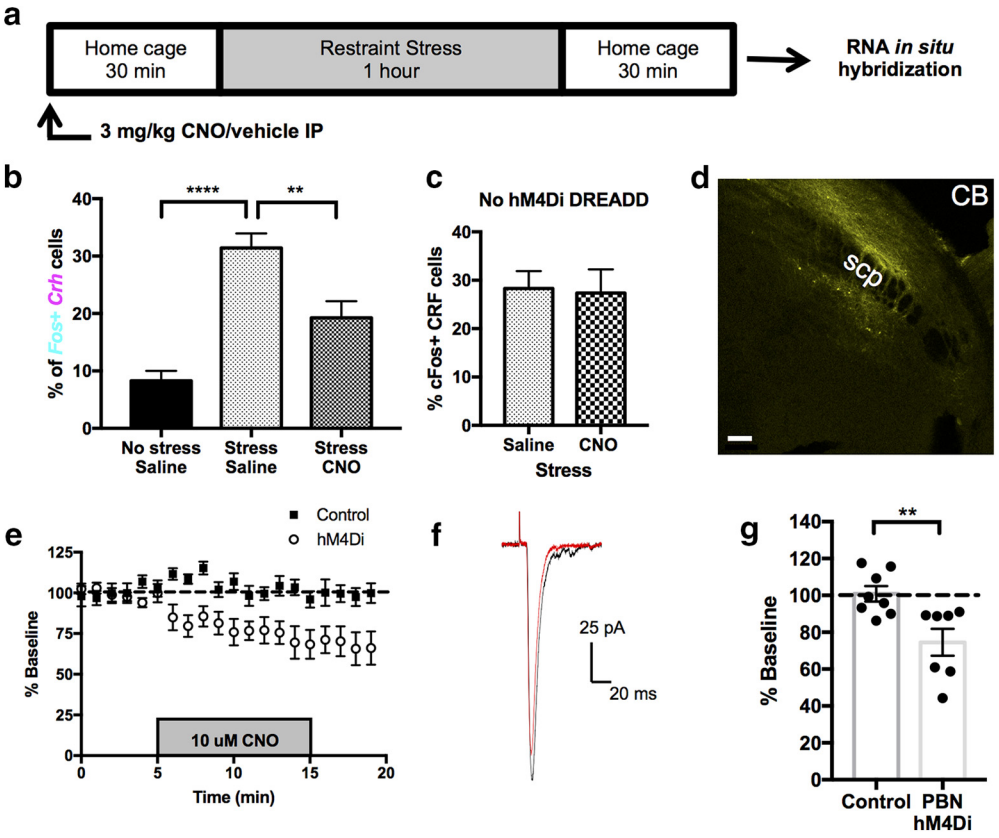

Figure 4. Activation of PBN-expressed Gi-coupled DREADD hM4Di blunts stress-induced *Fos* activation in *Crh* cells. ***a***, Schematic showing timeline of animal injection, restraint stress, and RNA *in situ* hybridization assay. ***b***, Summary bar graph showing effect of CNO injection on percentage of *Crh* cells that express *Fos* 30 min after restraint stress ($n = 10$ mice/group, 5 male/5 female; exception: no stress/saline $n = 9$). *Indicates significant difference between treatment groups (**$p < 0.01$, ****$p < 0.0001$). ***c***, Bar graph summarizing results of control immunohistochemistry experiment showing effect of CNO injection on male C57 mice (saline: $n = 4$; CNO: $n = 3$) with no hM4Di DREADD expression. ***d***, Example confocal image showing AAV5-hSyn-hM4D(Gi)-mCherry PBN injection site. Scale bar, 100 μm. scp, Superior cerebellar peduncle; CB, cerebellum. ***e***, Time course of CNO application on EPSC amplitude in BNST CRF cells, graphed as percentage of baseline, comparing control mice ($n = 8$ cells, $N = 2$ male, 2 female mice) and PBN hM4Di-expressing mice ($n = 7$ cells, $N = 1$ male, 1 female mouse). ***f***, Representative EPSC traces before (black) and after (red) CNO application in mice expressing PBN-hM4Di. ***g***, Summary bar graph showing average EPSC amplitude as a percentage of baseline during last 5 min of CNO application. *Indicates significant difference between control and hM4Di groups using unpaired *t* test (**$p < 0.01$). All data are represented as mean ± SEM.

activity, we recorded from tdtomato+ neurons in *ex vivo* slices containing the BNST while using electrical stimulation in the presence of picrotoxin to evoke EPSCs. We found that 10 min bath application of 10 μM CNO was able to reduce EPSC amplitude only in hM4Di injected animals (Fig. 4*e–g*). An unpaired *t* test comparing cells from control animals to cells from hM4Di-injected animals showed a significant decrease in EPSC amplitude in hM4Di animals during the last 5 min of CNO application (−25.5 ± 7.3% change from baseline, $p = 0.007$). A separate cohort of hM4Di-injected mice then underwent the same restraint stress paradigm as before, receiving an intraperitoneal injection of CNO (3 mg/kg) 30 min before the stressor (Fig. 4*a*). Using fluorescent *in situ* hybridization, we found that activation of the hM4Di DREADD significantly alters stress-induced *Fos* (Fig. 4*b*). A two-way ANOVA shows a significant effect of treatment ($F_{(2,23)} = 11.76$, $p < 0.001$), but no effect of sex ($F_{(1,23)} = 0.73$, $p = 0.401$) and no interaction ($F_{(2,23)} = 1.01$, $p = 0.380$). As there was no significant effect of sex, we have presented the male and female data combined (Fig. 4*b*). A one-way ANOVA reveals a significant effect of treatment ($F_{(2,26)} = 21.38$, $p < 0.0001$). *Post hoc* analysis using Sidak's multiple-comparisons test reveals a significant difference in percentage of *Fos*+ *Crh* cells between the stress/saline and stress/CNO mice (stress/saline: 31.4 ± 2.5%; stress/CNO: 19.2 ± 2.9%; $p = 0.0047$).

To rule out potential off-target actions of CNO, in a control experiment we assessed the effects of CNO alone without expression of the hM4Di DREADD on restraint stress-induced cFos expression in BNST CRF neurons (Fig. 4*c*). An unpaired *t* test found no change in the percentage of cFos+ CRF neurons across stress/saline and stress/CNO treatment (stress/saline: 28.3 ± 3.6%; stress/CNO: 27.4 ± 4.9%; $p = 0.878$). Together, these data show that activation of PBN-expressed hM4Di DREADD can mimic actions of guanfacine by decreasing stress-induced *Fos* activation in *Crh* cells.

Further definition of postsynaptic cell identity using Prkcd reveals a stress-sensitive increase in Prkcd/Crh coexpression in female mice

Based on knowledge of PKCδ neurons opposing actions to CRF cells in the fear response in the CeA (Haubensak et al., 2010; Asok et al., 2018), we hypothesized that PKCδ could similarly be an important marker in the BNST, and included *Prkcd* transcript analysis in our *in situ* hybridization assays (Fig. 5*b*). These studies revealed an interesting stress-sensitive sex difference. Following restraint stress, we observe a female-specific increase in the percentage of *Crh* neurons coexpressing *Prkcd* (Fig. 5*a*). Analysis by two-way ANOVA results in a significant effect of both stress ($F_{(1,15)} = 18.07$, $p = 0.001$) and sex ($F_{(1,15)} = 6.89$, $p = 0.019$), as

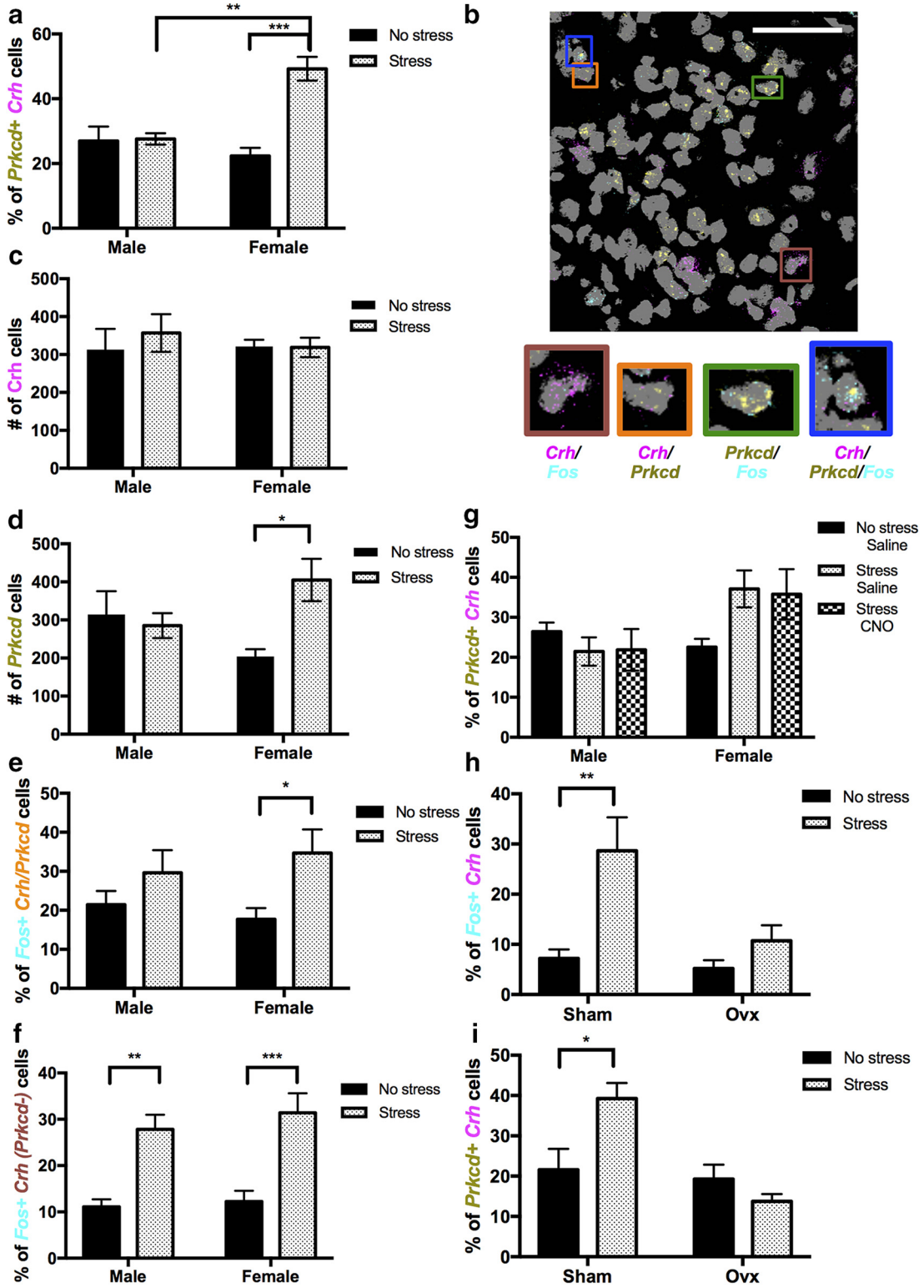

Figure 5. RNA *in situ* assay reveals a female-specific stress-induced increase in *Prkcd/Crh* coexpression that can be altered by ovariectomy. ***a***, Summary bar graph showing the percentage of *Crh* neurons that express *Fos* 30 min after restraint stress in male and female mice. *Indicates significant difference compared with each other group (**$p < 0.01$, ***$p < 0.001$). ***b***, Example image of RNA *in situ* assay (gray, DAPI-labeled nuclei; magenta, *Crh* transcripts; yellow, *Prkcd* transcripts; cyan, *Fos* transcripts). Boxes provide magnified examples of cells expressing multiple transcripts (maroon, *Crh/Fos*; orange, *Crh/Prkcd*; green, *Prkcd/Fos*; blue, *Crh/Prkcd/Fos*). ***c***, Summary bar graph showing the number of *Crh*-expressing cells 30 min after restraint stress in male and female mice. ***d***, Summary bar graph showing the number of *Prkcd*-expressing cells 30 min after restraint stress in male and female mice. *Indicates significant difference between stress conditions (*$p < 0.05$). ***e***, Summary bar graph showing the percentage of colocalized *Crh/Prkcd* cells that express *Fos* 30 min after restraint stress in male and female mice. *Indicates significant difference between stress conditions (*$p < 0.05$). ***f***, Summary bar graph showing the percentage of *Crh* cells (lacking *Prkcd*) that express *Fos* 30 min after restraint stress in male and female mice. *Indicates significant difference between stress conditions (**$p < 0.01$, ***$p < 0.001$). ***a–f***, Males: no stress $n = 5$, stress $n = 5$; Females: no stress $n = 5$, stress $n = 4$. g, Summary bar graph showing effect of CNO injection on percentage of *Crh* cells that express *Prkcd* 30 min after restraint stress in male and female mice ($n = 5$/mice per group; exception: female, no stress/saline $n = 4$). ***h***, ***i***, Summary bar graphs showing effect of ovariectomy on percentage of *Crh* cells that express *Fos* (***h***) or *Prkcd* (***i***) 30 min after restraint stress in female mice ($n = 5$ mice/group). *Indicates significant difference between stress conditions (**$p < 0.01$, *$p < 0.05$). All data are represented as mean ± SEM.

well as a significant interaction ($F_{(1,15)} = 16.43$, $p = 0.001$). *Post hoc* analysis using Tukey's multiple-comparisons test shows a significant increase in the percentage of *Crh* cells expressing *Prkcd* following stress in females (no stress: 22.3 ± 2.5%; stress: 49.3 ± 3.7%; $p < 0.001$), but no difference in males (no stress: 27 ± 4.4%; stress: 27.6 ± 1.8%; $p = 0.99$). This results in a significant difference between males and females following restraint stress ($p = 0.002$). To determine whether the coexpression of *Crh* and *Prkcd* in females after stress was because of an increase in *Crh* neurons or an increase in *Prkcd* neurons we looked at the overall number of neurons expressing these transcripts in the dBNST (Fig. 5*c*,*d*). A two-way ANOVA shows that *Crh* cell number remained unchanged throughout the experiment with no main effect of either stress ($F_{(1,15)} = 0.24$, $p = 0.629$) or sex ($F_{(1,15)} = 0.13$, $p = 0.724$), and no interaction ($F_{(1,15)} = 0.30$, $p = 0.589$). Conversely, total *Prkcd* cell number did not remain constant, as a two-way ANOVA reveals a significant interaction between stress and sex ($F_{(1,15)} = 6.68$, $p = 0.021$), but no main effect of either alone (sex: $F_{(1,15)} = 0.01$, $p = 0.920$; stress: $F_{(1,15)} = 3.70$, $p = 0.073$). *Post hoc* analysis with Tukey's multiple-comparisons test shows a significant increase in the number of *Prkcd* expressing cells in females following stress (no stress: 204 ± 19.2 cells; stress 405 ± 55.7 cells; $p = 0.033$), but not in males (no stress: 314.6 ± 61 cells; stress 285.2 ± 32.6 cells; $p = 0.962$). This suggests that *Prkcd* is being upregulated in *Crh*-expressing neurons and not vice versa.

To examine restraint stress activation of this newly identified neuronal population coexpressing *Crh*/*Prkcd*, we also looked at the presence of *Fos* transcripts in these neurons (Fig. 5*e*). When analyzing the percentage of *Crh*/*Prkcd* cells that contain *Fos*, a two-way ANOVA reveals a significant effect of stress ($F_{(1,15)} = 7.41$, $p = 0.016$), but no effect of sex ($F_{(1,15)} = 0.02$, $p = 0.889$) and no interaction ($F_{(1,15)} = 0.93$, $p = 0.353$). Sidak's multiple-comparisons test shows a significant increase in *Fos*+ *Crh/Prkcd* cells following stress in females (no stress: 17.7 ± 2.9%; stress: 34.7 ± 6.0%; $p = 0.046$), with no change in males (no stress: 21.5 ± 3.5%; stress: 29.6 ± 5.8%; $p = 0.389$). However, this *Crh/Prkcd* population in females only accounts for approximately one-half of the *Crh* cells, thus we also quantified *Fos* transcripts in *Crh* neurons that do not coexpress *Prkcd* (Fig. 5*f*). A two-way ANOVA shows a significant effect of stress ($F_{(1,15)} = 39.99$, $p < 0.0001$) on the percentage of *Fos*+ *Crh (Prkcd*-) cells, but no effect of sex ($F_{(1,15)} = 0.69$, $p = 0.418$) and no interaction ($F_{(1,15)} = 0.18$, $p = 0.675$). *Post hoc* analysis using Sidak's multiple-comparisons tests show a significant increase in *Fos*+ *Crh (Prkcd*-) cells following stress in both males (no stress: 11.1 ± 1.6%; stress: 27.8 ± 3.1%; $p = 0.001$) and females (no stress: 12.3 ± 2.3%; stress: 31.4 ± 4.2%; $p = 0.001$).

PBN hM4Di-dependent suppression of BNST CRF neuron Fos response is mechanistically distinct from the female-specific increase in Crh/Prkcd colocalization following stress

We next wanted to determine whether the stress-related increase in *Prkcd/Crh* in females could be blocked by PBN hM4Di activation. Unlike the decreased *Fos* response in Figure 4, hM4Di DREADD activation did not change the increase in coexpression of *Prkcd/Crh* in female mice after stress (Fig. 5*g*). A two-way ANOVA shows a significant effect of sex ($F_{(1,23)} = 5.60$, $p = 0.027$), but no effect of treatment ($F_{(2,23)} = 0.69$, $p = 0.512$) and no interaction ($F_{(2,23)} = 2.87$, $p = 0.077$). Tukey's multiple-comparisons test shows that there is no significant difference in percentage of *Prkcd*+ *Crh* cells between the stress/saline and stress/CNO mice in females (stress/saline: 37.1 ± 4.6%; stress/CNO: 35.8 ± 6.3%; $p = 0.973$). This suggests that while the increase in *Crh/Prkcd* colocalization in females is an interesting observation, it is mechanistically separate from effects observed following PBN hM4Di activation.

Stress-induced Fos activation of Crh cells and upregulation of Crh/Prkcd coexpression are both altered in ovariectomized mice

Finally, to begin to investigate a potential role for hormonal signaling related to the estrous cycle in BNST CRF neuron stress responsivity, we used ovariectomized (ovx) mice in our restraint stress paradigm. RNA *in situ* hybridization analysis shows that ovariectomy substantially reduces stress-induced *Fos* expression in dBNST *Crh* cells (Fig. 5*h*). A two-way ANOVA reveals a significant effect of both ovariectomy surgery ($F_{(1,16)} = 5.53$, $p = 0.032$) and stress ($F_{(1,16)} = 10.53$, $p = 0.005$), but no significant interaction ($F_{(1,16)} = 3.41$, $p = 0.083$). Tukey's multiple-comparison test shows that although stress still increases the percentage of *Fos*+ *Crh* cells in mice receiving a control sham surgery (no stress: 7.2 ± 1.8%; stress: 27.3 ± 6.8%; $p = 0.012$), those that underwent ovariectomy surgery no longer show a stress-induced *Fos* response in *Crh* cells (no stress: 5.2 ± 1.6%; stress 10.7 ± 3.1%; $p = 0.758$). Additionally, when analyzing *Prkcd*, we see that the stress-induced increase in *Crh/Prkcd* coexpression is also blocked in ovariectomized mice (Fig. 5*i*). Statistical analysis using two-way ANOVA shows a significant effect of ovariectomy surgery ($F_{(1,16)} = 11.71$, $p = 0.003$), but no significant effect of stress ($F_{(1,16)} = 1.86$, $p = 0.192$). However, there is a significant interaction between the variables ($F_{(1,16)} = 7.93$, $p = 0.012$). *Post hoc*, Tukey's multiple-comparisons show that mice that underwent sham surgery have a significant increase in *Crh/Prkcd* coexpression following stress (no stress: 21.6 ± 5.2%; stress: 37.6 ± 3.9%; $p = 0.042$). Conversely, ovariectomized mice no longer show a significant increase in *Crh/Prkcd* coexpressing cells (no stress: 19.3 ± 3.6%; stress: 13.7 ± 1.8%; $p = 0.736$). These results provide evidence for the involvement of sex hormones in the signaling pathways involved in the stress response of BNST CRF neurons.

Discussion

We find that restraint stress increases cFos expression in BNST CRF neurons, and that systemic administration of the clinically well tolerated drug guanfacine, an α_{2A}-AR agonist, reduces their activity. Using *ex vivo* electrophysiology, we demonstrated that NE inhibits excitatory input to these cells via α_2-AR activation, but that agonists for each class of AR produces modulation of excitatory drive, suggesting likely state-dependent actions *in vivo*. *Ex vivo* channelrhodopsin-assisted mapping identified the insular cortex and PBN as glutamatergic inputs to CRF cells, but only the PBN was sensitive to NE and guanfacine modulation. Further, CNO activation of PBN-expressed Gi-coupled DREADDs (hM4Di) was able to mimic actions of guanfacine by decreasing stress-induced *Fos* in *Crh* neurons. Finally, defining BNST cell populations using *Prkcd* uncovered a unique population of BNST *Crh* neurons in female mice.

Stress-induced activation of BNST CRF neurons

Anxiogenic stimuli have been shown to induce cFos expression in CRF neurons throughout the BNST in both mice and rats (Butler et al., 2016; Lin et al., 2018) suggesting that, despite known anatomical differences in the CRF systems of rodents (Daniel et al., 2017), increased CRF activation in the BNST following aversive stimuli may be an important conserved signal. We found both

males and females exhibited increased cFos+ CRF neurons in response to stress and both were sensitive to regulation by systemic guanfacine administration. Interestingly, guanfacine was able to alter cFos expression in the no stress condition, showing that guanfacine actions do not require stress activation of these neurons. Substantial evidence has demonstrated sex differences within the CRF system, both at the level of the HPA axis and at extrahypothalamic sites (Bangasser and Valentino, 2014). In rats, females have been shown to have higher numbers of CRF cells in the vBNST, as well as increased colocalization with *Fos* following stress (Babb et al., 2013). While our study did not reveal sex differences in restraint stress-induced *Crh/Fos* colocalization in dBNST neurons, we did find that this response could be blocked in ovariectomized females, providing further evidence that hormonal signaling is an important aspect of BNST stress responsivity.

Norepinephrine modulation of excitatory drive onto CRF neurons

Our experiments provide insight into the specific mechanisms underlying systemic guanfacine regulation of stress-induced cFos expression in BNST CRF neurons. Stress has been shown to increase NE signaling within the BNST (Pacak et al., 1995) and previous work has shown that isoproterenol, a β-AR agonist, can increase glutamatergic transmission in the BNST via a CRF receptor-dependent mechanism and can depolarize BNST CRF neurons (Nobis et al., 2011; Silberman et al., 2013). We showed that isoproterenol can increase glutamatergic drive onto CRF neurons, likely through postsynaptic actions. Conversely, the stimulation of α-ARs works in opposition to regulate CRF neuron activity. Although NE and methoxamine did not alter PPR, guanfacine was able to alter this ratio, suggesting that NE can potentially regulate excitatory input postsynaptically by actions of α_1-ARs as well as presynaptically by α_{2a}-ARs located on glutamatergic terminals presynaptic to CRF cells. Specifically blocking α_2-ARs with atipamezole completely inhibited the actions of NE and in some cells uncovered possible NE actions at β-ARs. A trend toward a similar phenomenon was recently reported in a population of vBNST neurons as well (Gungor et al., 2018). These results, in combination with the systemic effects of guanfacine administration, suggest that the balance between NE activation of β- and α-ARs may be key in controlling the response of CRF neurons to stress. These results led us to focus on α_2-AR signaling, but future studies are needed to tease apart the contribution of α_1-AR and β-AR signaling in regulating CRF neurons.

We identified two excitatory inputs to CRF neurons using optogenetic stimulation: the insula and the PBN. We observed differential oEPSC kinetics from the insula and PBN stimulations. The slower kinetics of the insular input could suggest an axo-dendritic synapse, whereas the faster PBN kinetics and CGRP immunohistochemistry findings agree with known axo-somatic connections in the BNST (Shimada et al., 1989; Dobolyi et al., 2005). While overall the kinetics observed are slower than those seen with electrical stimulation, the same optical stimulation protocol was used for both inputs, allowing for direct comparison.

We found that NE and guanfacine could inhibit the PBN input, while the insula input was insensitive. This finding is similar to previous work showing that the PBN input to unidentified BNST neurons can be inhibited by guanfacine, while the basolateral amygdala input was insensitive (Flavin et al., 2014). This suggests that the actions of NE on CRF cells are at least in part working through α_{2A}-ARs on PBN terminals presynaptic to CRF cells. Previous studies in the CeA have suggested that α_{2A}-ARs decrease PBN release probability by directly interacting with the release machinery (Delaney et al., 2007). The input selectivity of NE regulation demonstrates that targeting this system produces highly specific tailoring of excitatory drive to the BNST.

Modulation of PBN activity using the Gi-coupled DREADD hM4Di

Having identified the PBN as a guanfacine-sensitive input to BNST CRF neurons, we further explored the regulation of this input in BNST stress responses, particularly given recent findings that the PBN encodes danger signals (Campos et al., 2018). We showed that activation of the Gi-coupled DREADD hM4Di in PBN neurons could mimic actions of guanfacine by decreasing stress-induced *Fos* in *Crh* neurons. Similar to the effect observed with guanfacine, our PBN manipulation was effective in blocking the CRF neuron stress response. However, α_{2A}-ARs are expressed in multiple compartments throughout the BNST and not just at PBN terminals (Flavin et al., 2014). Although we have shown the insular input to be insensitive to NE, guanfacine could be inhibiting other glutamatergic inputs to the BNST. For example, the paraventricular thalamus has been implicated in extended amygdala fear circuitry (Myers et al., 2014; Penzo et al., 2015). Additionally, there are other modulatory systems recruited by stress that may contribute to activation. Serotonin is known to play a role in promoting anxiety and can activate CRF neurons (Marcinkiewcz et al., 2016). Dynorphin actions at κ opioid receptors have been shown to inhibit anxiolytic circuitry in the BNST (Crowley et al., 2016). Alternatively, decreases in neuropeptide Y signaling following stress could increase CRF neuron activation (Pleil et al., 2015). Better understanding differences in guanfacine actions at specific inputs and cellular compartments will aid in developing more effective drugs targeting the norepinephrine system.

A unique population of BNST CRF neurons in females

Although using PKCδ as a marker to further dissect the heterogeneous BNST did not explain the sex-specific response to activation of PBN-expressed hM4Di, it did uncover an additional sex difference in the BNST stress response. We found that expression of *Crh* and *Prkcd* desegregated in females after stress. As this coexpressing population of neurons also show a stress-induced *Fos* response, it is possible that this population marks a uniquely stress-sensitive population of neurons in the female. *Prkcd* has an estrogen response element and can be regulated by estrogen signaling in other systems (Shanmugam et al., 1999). The ability of ovariectomy to block this increase in coexpression supports the role of estrogen in this response. Additionally, PKCδ signaling has been linked to neuroinflammatory responses, which can be activated by stress (Ghayur et al., 1996; Anantharam et al., 2002), making this newfound population of neurons in the female BNST an interesting target for future studies.

Together, our results have led us to propose a model by which activation of α_{2A}-AR signaling in the BNST can decrease activation of BNST CRF neurons. While stress increases NE release that can act at many different receptor subclasses throughout the BNST, specifically targeting α_{2A}-ARs located on PBN terminals presynaptic to CRF cells can decrease activation of these cells. In conclusion, these findings provide a framework for understanding how the interaction between NE and glutamatergic signaling can modulate stress responsivity of BNST CRF neurons. We have identified both molecular and circuit-specific targets for addressing the pathophysiology underlying stress-related psychiatric

disorders. Additionally, we have uncovered a female-specific stress-sensitive population of neurons in the BNST, providing further evidence of mechanistic differences in the stress response between males and females. Future studies will further dissect the input specificity of this stress response, while continuing to focus on sex differences within the system to better identify targets for manipulating this stress circuitry.

References

Anantharam V, Kitazawa M, Wagner J, Kaul S, Kanthasamy AG (2002) Caspase-3-dependent proteolytic cleavage of protein kinase Cδ is essential for oxidative stress-mediated dopaminergic cell death after exposure to methylcyclopentadienyl manganese tricarbonyl. J Neurosci 22:1738–1751. CrossRef Medline

Asok A, Draper A, Hoffman AF, Schulkin J, Lupica CR, Rosen JB (2018) Optogenetic silencing of a corticotropin-releasing factor pathway from the central amygdala to the bed nucleus of the stria terminalis disrupts sustained fear. Mol Psychiatry 23:914–922. CrossRef Medline

Babb JA, Masini CV, Day HE, Campeau S (2013) Sex differences in activated corticotropin-releasing factor neurons within stress-related neurocircuitry and hypothalamic–pituitary–adrenocortical axis hormones following restraint in rats. Neuroscience 234:40–52. CrossRef Medline

Bangasser DA, Valentino RJ (2014) Sex differences in stress-related psychiatric disorders: neurobiological perspectives. Front Neuroendocrinol 35:303–319. CrossRef Medline

Butler RK, Oliver EM, Sharko AC, Parilla-Carrero J, Kaigler KF, Fadel JR, Wilson MA (2016) Activation of corticotropin releasing factor-containing neurons in the rat central amygdala and bed nucleus of the stria terminalis following exposure to two different anxiogenic stressors. Behav Brain Res 304:92–101. CrossRef Medline

Campos CA, Bowen AJ, Roman CW, Palmiter RD (2018) Encoding of danger by parabrachial CGRP neurons. Nature 555:617–622. CrossRef Medline

Carter ME, Soden ME, Zweifel LS, Palmiter RD (2013) Genetic identification of a neural circuit that suppresses appetite. Nature 503:111–114. CrossRef Medline

Carter ME, Han S, Palmiter RD (2015) Parabrachial calcitonin gene-related peptide neurons mediate conditioned taste aversion. J Neurosci 35:4582–4586. CrossRef Medline

Casada JH, Dafny N (1991) Restraint and stimulation of bed nucleus of the stria terminalis produce similar stress-like behaviors. Brain Res Bull 27:207–212. CrossRef Medline

Chen Q, Roeder Z, Li MH, Zhang Y, Ingram SL, Heinricher MM (2017) Optogenetic evidence for a direct circuit linking nociceptive transmission through the parabrachial complex with pain-modulating neurons of the rostral ventromedial medulla (RVM). eNeuro 4:ENEURO.0202–17.2017. CrossRef Medline

Chen Y, Molet J, Gunn BG, Ressler K, Baram TZ (2015) Diversity of reporter expression patterns in transgenic mouse lines targeting corticotropin-releasing hormone-expressing neurons. Endocrinology 156:4769–4780. CrossRef Medline

Choi DC, Nguyen MM, Tamashiro KL, Ma LY, Sakai RR, Herman JP (2006) Chronic social stress in the visible burrow system modulates stress-related gene expression in the bed nucleus of the stria terminalis. Physiol Behav 89:301–310. CrossRef Medline

Chrousos GP (2009) Stress and disorders of the stress system. Nat Rev Endocrinol 5:374–381. CrossRef Medline

Crestani CC, Alves FH, Gomes FV, Resstel LB, Correa FM, Herman JP (2013) Mechanisms in the bed nucleus of the stria terminalis involved in control of autonomic and neuroendocrine functions: a review. Curr Neuropharmacol 11:141–159. CrossRef Medline

Crowley NA, Bloodgood DW, Hardaway JA, Kendra AM, McCall JG, Al-Hasani R, McCall NM, Yu W, Schools ZL, Krashes MJ, Lowell BB, Whistler JL, Bruchas MR, Kash TL (2016) Dynorphin controls the gain of an amygdalar anxiety circuit. Cell Rep 14:2774–2783. CrossRef Medline

Daniel SE, Guo J, Rainnie DG (2017) A comparative analysis of the physiological properties of neurons in the anterolateral bed nucleus of the stria terminalis in the mus musculus, rattus norvegicus, and macaca mulatta. J Comp Neurol 525:2235–2248. CrossRef Medline

Delaney AJ, Crane JW, Sah P (2007) Noradrenaline modulates transmission at a central synapse by a presynaptic mechanism. Neuron 56:880–892. CrossRef Medline

Dobolyi A, Irwin S, Makara G, Usdin TB, Palkovits M (2005) Calcitonin gene-related peptide-containing pathways in the rat forebrain. J Comp Neurol 489:92–119. CrossRef Medline

Egli RE, Kash TL, Choo K, Savchenko V, Matthews RT, Blakely RD, Winder DG (2005) Norepinephrine modulates glutamatergic transmission in the bed nucleus of the stria terminalis. Neuropsychopharmacology 30:657–668. CrossRef Medline

Fadok JP, Krabbe S, Markovic M, Courtin J, Xu C, Massi L, Botta P, Bylund K, Müller C, Kovacevic A, Tovote P, Lüthi A (2017) A competitive inhibitory circuit for selection of active and passive fear responses. Nature 542:96–100. CrossRef Medline

Flavin SA, Matthews RT, Wang Q, Muly EC, Winder DG (2014) α_{2A}-Adrenergic receptors filter parabrachial inputs to the bed nucleus of the stria terminalis. J Neurosci 34:9319–9331. CrossRef Medline

Franklin KB, Paxinos G (2007) The mouse brain in stereotaxic coordinates. New York: Elsevier.

Funk CK, O'Dell LE, Crawford EF, Koob GF (2006) Corticotropin-releasing factor within the central nucleus of the amygdala mediates enhanced ethanol self-administration in withdrawn, ethanol-dependent rats. J Neurosci 26:11324–11332. CrossRef Medline

Ghayur T, Hugunin M, Talanian RV, Ratnofsky S, Quinlan C, Emoto Y, Pandey P, Datta R, Huang Y, Kharbanda S, Allen H, Kamen R, Wong W, Kufe D (1996) Proteolytic activation of protein kinase Cδ by an ICE/CED 3-like protease induces characteristics of apoptosis. J Exp Med 184:2399–2404. CrossRef Medline

Gungor NZ, Yamamoto R, Pare D (2018) Glutamatergic and GABAergic ventral BNST neurons differ in their physiological properties and responsiveness to noradrenaline. Neuropsychopharmacology 43:2126–2133. CrossRef Medline

Haubensak W, Kunwar PS, Cai H, Ciocchi S, Wall NR, Ponnusamy R, Biag J, Dong HW, Deisseroth K, Callaway EM, Fanselow MS, Luthi A, Anderson DJ (2010) Genetic dissection of an amygdala microcircuit that gates conditioned fear. Nature 468:270–276. CrossRef Medline

Koob GF (1999) Corticotropin-releasing factor, norepinephrine, and stress. Biol Psychiatry 46:1167–1180. CrossRef Medline

Krawczyk M, Georges F, Sharma R, Mason X, Berthet A, Bezard E, Dumont EC (2011) Double-dissociation of the catecholaminergic modulation of synaptic transmission in the oval bed nucleus of the stria terminalis. J Neurophysiol 105:145–153. CrossRef Medline

Lin X, Itoga CA, Taha S, Li MH, Chen R, Sami K, Berton F, Francesconi W, Xu X (2018) c-fos mapping of brain regions activated by multi-modal and electric foot shock stress. Neurobiol Stress 8:92–102. CrossRef Medline

Mantsch JR, Weyer A, Vranjkovic O, Beyer CE, Baker DA, Caretta H (2010) Involvement of noradrenergic neurotransmission in the stress- but not cocaine-induced reinstatement of extinguished cocaine-induced conditioned place preference in mice: role for beta-2 adrenergic receptors. Neuropsychopharmacology 35:2165–2178. CrossRef Medline

Marcinkiewcz CA, Mazzone CM, D'Agostino G, Halladay LR, Hardaway JA, DiBerto JF, Navarro M, Burnham N, Cristiano C, Dorrier CE, Tipton GJ, Ramakrishnan C, Kozicz T, Deisseroth K, Thiele TE, McElligott ZA, Holmes A, Heisler LK, Kash TL (2016) Serotonin engages an anxiety and fear-promoting circuit in the extended amygdala. Nature 537:97–101. CrossRef Medline

McDonald AJ, Shammah-Lagnado SJ, Shi C, Davis M (1999) Cortical afferents to the extended amygdala. Ann N Y Acad Sci 877:309–338. CrossRef Medline

McElligott ZA, Klug JR, Nobis WP, Patel S, Grueter BA, Kash TL, Winder DG (2010) Distinct forms of gq-receptor-dependent plasticity of excitatory transmission in the BNST are differentially affected by stress. Proc Natl Acad Sci U S A 107:2271–2276. CrossRef Medline

Myers B, Mark Dolgas C, Kasckow J, Cullinan WE, Herman JP (2014) Central stress-integrative circuits: forebrain glutamatergic and GABAergic projections to the dorsomedial hypothalamus, medial preoptic area, and bed nucleus of the stria terminalis. Brain Struct Funct 219:1287–1303. CrossRef Medline

Nobis WP, Kash TL, Silberman Y, Winder DG (2011) beta-adrenergic receptors enhance excitatory transmission in the bed nucleus of the stria terminalis through a corticotrophin-releasing factor receptor-dependent and cocaine-regulated mechanism. Biol Psychiatry 69:1083–1090. CrossRef Medline

Olsen CM, Winder DG (2010) Operant sensation seeking in the mouse. J Vis Exp 45:e2292. CrossRef Medline

Pacak K, McCarty R, Palkovits M, Kopin IJ, Goldstein DS (1995) Effects of immobilization on in vivo release of norepinephrine in the bed nucleus of the stria terminalis in conscious rats. Brain Res 688:242–246. CrossRef Medline

Penzo MA, Robert V, Tucciarone J, De Bundel D, Wang M, Van Aelst L, Darvas M, Parada LF, Palmiter RD, He M, Huang ZJ, Li B (2015) The paraventricular thalamus controls a central amygdala fear circuit. Nature 519:455–459. CrossRef Medline

Pleil KE, Rinker JA, Lowery-Gionta EG, Mazzone CM, McCall NM, Kendra AM, Olson DP, Lowell BB, Grant KA, Thiele TE, Kash TL (2015) NPY signaling inhibits extended amygdala CRF neurons to suppress binge alcohol drinking. Nat Neurosci 18:545–552. CrossRef Medline

Sallee FR, Lyne A, Wigal T, McGough JJ (2009) Long-term safety and efficacy of guanfacine extended release in children and adolescents with attention-deficit/hyperactivity disorder. J Child Adolesc Psychopharmacol 19:215–226. CrossRef Medline

Sanford CA, Soden ME, Baird MA, Miller SM, Schulkin J, Palmiter RD, Clark M, Zweifel LS (2017) A central amygdala CRF circuit facilitates learning about weak threats. Neuron 93:164–178. CrossRef Medline

Sato M, Ito M, Nagase M, Sugimura YK, Takahashi Y, Watabe AM, Kato F (2015) The lateral parabrachial nucleus is actively involved in the acquisition of fear memory in mice. Mol Brain 8:22. CrossRef Medline

Shaham Y, Highfield D, Delfs J, Leung S, Stewart J (2000) Clonidine blocks stress-induced reinstatement of heroin seeking in rats: an effect independent of locus coeruleus noradrenergic neurons. Eur J Neurosci 12:292–302. CrossRef Medline

Shanmugam M, Krett NL, Maizels ET, Cutler RE Jr, Peters CA, Smith LM, O'Brien ML, Park-Sarge OK, Rosen ST, Hunzicker-Dunn M (1999) Regulation of protein kinase Cδ by estrogen in the MCF-7 human breast cancer cell line. Mol Cell Endocrinol 148:109–118. CrossRef Medline

Shields AD, Wang Q, Winder DG (2009) alpha2A-adrenergic receptors heterosynaptically regulate glutamatergic transmission in the bed nucleus of the stria terminalis. Neuroscience 163:339–351. CrossRef Medline

Shimada S, Inagaki S, Kubota Y, Kito S, Funaki H, Takagi H (1989) Light and electron microscopic studies of calcitonin gene-related peptide-like immunoreactive terminals in the central nucleus of the amygdala and the bed nucleus of the stria terminalis of the rat. Exp Brain Res 77:217–220. Medline

Silberman Y, Matthews RT, Winder DG (2013) A corticotropin releasing factor pathway for ethanol regulation of the ventral tegmental area in the bed nucleus of the stria terminalis. J Neurosci 33:950–960. CrossRef Medline

Sterrenburg L, Gaszner B, Boerrigter J, Santbergen L, Bramini M, Roubos EW, Peeters BW, Kozicz T (2012) Sex-dependent and differential responses to acute restraint stress of corticotropin-releasing factor-producing neurons in the rat paraventricular nucleus, central amygdala, and bed nucleus of the stria terminalis. J Neurosci Res 90:179–192. CrossRef Medline

Sullivan GM, Apergis J, Bush DE, Johnson LR, Hou M, Ledoux JE (2004) Lesions in the bed nucleus of the stria terminalis disrupt corticosterone and freezing responses elicited by a contextual but not by a specific cue-conditioned fear stimulus. Neuroscience 128:7–14. CrossRef Medline

Tran L, Schulkin J, Greenwood-Van Meerveld B (2014) Importance of CRF receptor-mediated mechanisms of the bed nucleus of the stria terminalis in the processing of anxiety and pain. Neuropsychopharmacology 39:2633–2645. CrossRef Medline

Wang X, Cen X, Lu L (2001) Noradrenaline in the bed nucleus of the stria terminalis is critical for stress-induced reactivation of morphine-conditioned place preference in rats. Eur J Pharmacol 432:153–161. CrossRef Medline